Liquid Crystals
Publication details, including instructions for authors and subscription information:
http://www.informaworld.com/smpp/title~content=t713926090

Blue phase III widening in CE6-dispersed surface-functionalised CdSe nanoparticles

George Cordoyiannis[ab]; Patricia Losada-Pérez[a]; Chandra Shekhar Pati Tripathi[a]; Brigita Rožič[b]; Uroš Tkalec[b]; Vassilios Tzitzios[c]; Eva Karatairi[cd]; George Nounesis[c]; Zdravko Kutnjak[b]; Igor Muševič[b]; Christ Glorieux[a]; Samo Kralj[be]; Jan Thoen[a]
[a] Departement Natuurkunde en Sterrenkunde, Katholieke Universiteit Leuven, Laboratorium voor Akoestiek en Thermische Fysica, Leuven, Belgium [b] Condensed Matter Physics Department, Jožef Stefan Institute, Ljubljana, Slovenia [c] National Centre for Scientific Research 'Demokritos', Aghia Paraskevi, Greece [d] Department of Materials Science, University of Patras, Patras, Greece [e] Department of Physics, University of Maribor, Maribor, Slovenia

Online publication date: 15 November 2010

To cite this Article Cordoyiannis, George , Losada-Pérez, Patricia , Tripathi, Chandra Shekhar Pati , Rožič, Brigita , Tkalec, Uroš , Tzitzios, Vassilios , Karatairi, Eva , Nounesis, George , Kutnjak, Zdravko , Muševič, Igor , Glorieux, Christ , Kralj, Samo and Thoen, Jan(2010) 'Blue phase III widening in CE6-dispersed surface-functionalised CdSe nanoparticles', Liquid Crystals, 37: 11, 1419 — 1426
To link to this Article: DOI: 10.1080/02678292.2010.519057
URL: http://dx.doi.org/10.1080/02678292.2010.519057

Liquid Crystals,
Vol. 37, No. 11, November 2010, 1419–1426

Taylor & Francis
Taylor & Francis Group

Blue phase III widening in CE6-dispersed surface-functionalised CdSe nanoparticles

George Cordoyiannis[a,b*], Patricia Losada-Pérez[a], Chandra Shekhar Pati Tripathi[a], Brigita Rožič[b], Uroš Tkalec[b], Vassilios Tzitzios[c], Eva Karatairi[c,d], George Nounesis[c], Zdravko Kutnjak[b], Igor Muševič[b], Christ Glorieux[a], Samo Kralj[b,e] and Jan Thoen[a]

[a]*Laboratorium voor Akoestiek en Thermische Fysica, Departement Natuurkunde en Sterrenkunde, Katholieke Universiteit Leuven, Leuven, Belgium;* [b]*Condensed Matter Physics Department, Jožef Stefan Institute, Ljubljana, Slovenia;* [c]*National Centre for Scientific Research 'Demokritos', Aghia Paraskevi, Greece;* [d]*Department of Materials Science, University of Patras, Patras, Greece;* [e]*Department of Physics, University of Maribor, Maribor, Slovenia*

(*Received 28 May 2010; final version received 24 August 2010*)

The phase transition behaviour of the chiral liquid crystal CE6 doped with spherical surface-functionalised CdSe nanoparticles has been examined by means of high-resolution adiabatic scanning calorimetry and polarising microscopy. The addition of nanoparticles results in an essentially stabilised blue phase III. The phase diagram is displayed upon heating and cooling and the enthalpy changes involved in the conversion between the blue phases are determined. The dispersion of functionalised nanoparticles is prominent for the stabilisation of blue phase III, which is potentially useful for applications, especially if applied on liquid crystals that exhibit blue phases close to room temperature.

Keywords: adiabatic scanning calorimetry; polarising microscopy; liquid crystals; blue phases; nanoparticles

1. Introduction

More than one century ago, in his famous article on the properties of cholesterol, F. Reinitzer reported splendid colour phenomena occurring before the solidification of cholesteryl acetate and other cholesterol derivatives [1]. What Reinitzer observed as reflections of green, changing to blue in a sample sandwiched between glass plates was the presence of the, unknown at that time, blue phases (BPs). BPs exist within a narrow temperature range between the isotropic (I) and the cholesteric or chiral nematic (N*) phase of some chiral liquid crystals [2]. In order of decreasing temperature, three distinct BPs appear, which are classified as blue phase III (BPIII), blue phase II (BPII) and blue phase I (BPI). The BPIII is amorphous, while the BPII and BPI possess simple cubic and body-centred cubic symmetry, respectively [3–6]. These phases have been extensively studied both experimentally, by means of optical [7, 8] and calorimetric techniques [9, 10], and theoretically [11–15]. In addition, phase diagrams have been proposed as a function of chirality. The strength of chirality holds a key role for the existence of a critical point of liquid-gas type in the I–BPIII phase transition [16–18]. Besides the fundamental aspects and critical phenomena, BPs exhibit an exceptional potential for applications in photonics and the display industry [19–21]. Nevertheless, their use is hampered due to the narrow temperature range in which they usually appear. As a consequence, the stabilisation of BPs has been the subject of a broad research interest for several years, in terms of both experimental and theoretical studies [22–32].

Very recently, a pure compound with a wide-range BPIII has been reported, albeit only on cooling [33, 34]. Simultaneously, various efforts have been made to stabilise the BPs in mixtures of liquid crystals and various types of nanoparticles, such as Au, CdSe and aerosils [35, 36]. In this paper we report on the experimental results of several mixtures composed of a chiral liquid crystal and CdSe nanoparticles. High-resolution adiabatic scanning calorimetry (ASC) and optical polarising microscopy have been applied for a systematic study of these mixtures. It is demonstrated that the BPIII is greatly stabilised by the presence of nanoparticles, while the BPII gradually disappears and the BPI is rather weakly affected.

2. Materials and methods

The liquid crystal S-(+)-4-(2-methylbutyl)phenyl-4-decyloxybenzoate (CE6) was supplied by BDH, UK, stored carefully and used without any further treatment. It exhibits all three BPs and, moreover, a smectic A (SmA) phase prior to crystallisation. The chemical formula of CE6 is shown in the top part of Figure 1. As a guide for its transition temperatures we have used the data of previous pure CE6 measurements by

*Corresponding author. Email: george.cordoyiannis@ijs.si

ISSN 0267-8292 print/ISSN 1366-5855 online

DOI: 10.1080/02678292.2010.519057
http://www.informaworld.com

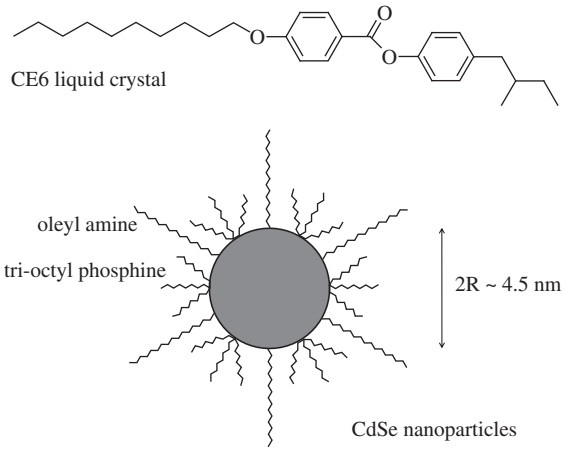

Figure 1. The chemical formula of the liquid crystal CE6 is presented in the top part. In the bottom part, a simple schematic representation of the CdSe nanoparticles surface-treated with oleyl amine and tri-octyl phosphine is shown. The diameter of the nanoparticles core is $2R \sim 4.5$ nm.

means of optical microscopy [37] and ASC [38]. The CdSe nanoparticles were synthesised at the National Centre for Scientific Research 'Demokritos'. They are of spherical shape and have an average diameter $2R \sim 4.5$ nm. Their surface was treated with hydrophobic oleyl amine and tri-octyl phosphine. A simple schematic representation of these particles is given in the bottom part of Figure 1, while details on their synthesis can be found elsewhere [39]. They are well dispersed in non-polar solvents such us toluene and they exhibit a narrow size distribution as has been confirmed by transmission electron microscopy measurements [36, 39].

Apart from the pure CE6, several mixtures with CdSe nanoparticles were prepared, namely $x = 0.0005$, 0.005 and 0.02, where x is the ratio of the mass of nanoparticles to the mass of CE6. Prior to preparation of the mixture, the solution (in toluene) of the CdSe nanoparticles was inserted in an ultrasonic bath for 1 h to eliminate any possible aggregation. Afterwards, the liquid crystal and the nanoparticles were thoroughly mixed for at least 3 days in highly pure toluene, by continuous stirring and periodical sonification of the solution. After the toluene had fully evaporated, the samples were placed in the calorimetric cells.

Heating and cooling runs on pure CE6 and on all mixtures were carried out using high-resolution ASC. The ASC apparatus was fully computerised and consisted of four stages, the first being the sample cell and the other three the surrounding shields. For the current measurements the inner stage was a 22 g tantalum cell, which contained approximately 1.7 g of sample. The heat capacity of the empty cell was measured in a separate control experiment. It was then subtracted from the total heat capacity (of the sample and cell) and the result was divided by the sample mass in order to derive the net specific heat capacity of the sample. Apart from the sample, the cell also contained a stirring ball made of stainless steel. By continuously changing the inclination of the apparatus during the experiment, the stirring ball moved back and forth in order to maintain the homogeneity of the mixture and to eliminate any temperature gradients within the sample. In order to reduce the thermal coupling between the various stages and attain optimal thermal insulation, the space between the cell and the three surrounding shields was vacuum-pumped.

In ASC, very slow scanning rates can be achieved. In the principal mode of operation (heating or cooling), each run yields the temperature dependence of both the heat capacity C_p and the enthalpy H. ASC can easily distinguish between continuous (second-order) and discontinuous (first-order) transitions. One important feature of this technique is that in its principal mode of operation it applies a constant heating or cooling power instead of a constant scanning rate. This leads to a substantial decrease of the scanning rate in the coexistence region of a first-order transition, since the applied power is dissipated not only for the temperature change of the sample but also for the change between the two coexisting phases. The decrease of the scanning rate provides excellent resolution data and the latent heat can be accurately determined when present. The precision of the technique is better than 2 mJ g^{-1}; hence, it is ideal for studies of BPs that involve small heat transitions and the reproduction of the respective phase diagrams. A more detailed description of ASC can be found elsewhere [40, 41].

Complementary microscopic observations were performed in order to obtain images of the BPs of pure CE6 and one of the larger CdSe concentration. A Nikon Eclipse E600 polarising microscope and a Pixelink PL-A741 camera were used. For these measurements the samples were sandwiched between glass plates, and then placed on an Instec model STC-200 heating stage with a temperature stability of 0.1 K and, subsequently, examined under crossed polarisers.

3. Results and discussion

A bulk CE6 sample has previously been studied in a similar calorimeter [38, 42]. In order to confirm the good condition of the present sample, a slow heating run was performed in the vicinity of BPs, yielding data that demonstrate very sharp first-order transitions occurring at the same temperatures as previously recorded. The heat capacity temperature profile $C_p(T)$ in the vicinity of the BPs of the bulk CE6 is presented in Figure 2. The N*–BPI, BPI–BPII, BPII–BPIII and BPIII–I transition peaks can be clearly distinguished

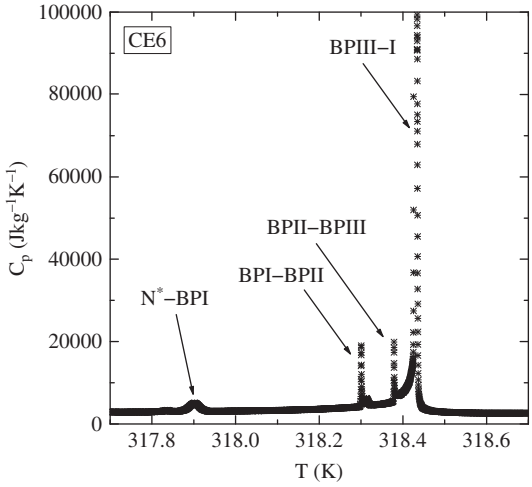

Figure 2. The heat capacity temperature profile $C_p(T)$ for a heating run of pure CE6 in the vicinity of BPs. From left to right (i.e. on increasing the temperature) the N*–BPI, BPI–BPII, BPII–BPIII and BPIII–I phase transitions can be seen. A slow scanning rate of 0.019 K h^{-1} was used.

upon raising the temperature. Due to the first-order character of these transitions, very high effective heat capacity values are observed in this figure. Afterwards, the mixtures of the above-mentioned concentrations were measured on cooling and heating. First, a cooling run was performed down to the SmA phase and then a slower heating run was carried out in a short temperature range to obtain high-resolution data allowing for a precise determination of the enthalpy changes related to BPs. In Table 1 information on the type of run and the scanning rate is given for the measurements of pure CE6 and its mixtures with CdSe nanoparticles.

In Figure 3 the $C_p(T)$ profiles are shown for the cooling runs of the mixtures $x = 0.0005$, 0.005 and 0.02. In this figure all the data are plotted in the same scale in order to compare the effect of various CdSe concentrations on the phase transitions. The insets show a 'blow up' of the heat capacity profiles in the vicinity of the BPs, illustrating the details that cannot

Table 1. The features of all runs performed on pure CE6 and on mixtures with CdSe nanoparticles.

Concentration	Type of run	Scanning rate[a] (K h^{-1})
$x = 0$	heating	0.019
$x = 0.0005$	cooling	0.104
$x = 0.005$	cooling	0.109
	heating	0.027
$x = 0.02$	cooling	0.109
	heating	0.019

Note: [a]Scanning rate refers to the average rate, since in the phase-coexistence region the scanning rate slows down.

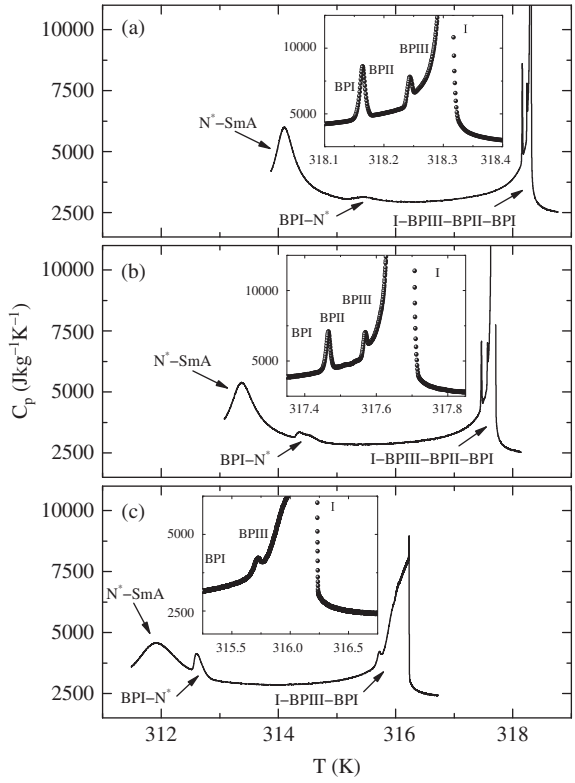

Figure 3. The $C_p(T)$ profiles for all of the cooling runs performed on CE6 and CdSe mixtures, with (a) $x = 0.0005$, (b) $x = 0.005$ and (c) $x = 0.02$ on the same scale. The inset in each plot shows a 'close up' of the data in the vicinity of BPs.

be clearly seen in a full-range plot. When increasing the nanoparticle concentration in the mixtures, all the transitions are shifted to lower temperatures and they gradually become more smeared and broadened (apart from the BPI–N* transition as we will discuss below). The range of BPIII is systematically widened as a function of CdSe concentration. BPII is present and weakly affected for $x = 0.0005$ and 0.005, while it is not observed for the $x = 0.02$ sample (i.e. it disappears somewhere between $x = 0.005$ and 0.02). The range of BPI is widened even by the presence of a small number of nanoparticles ($x \leq 0.005$), but this influence weakens for the higher concentration ($x = 0.02$). Nevertheless, as will be explained later, by comparing the cooling with the heating runs, this widening can be attributed to supercooling effects.

The BPI–N* phase transition is an exception to the general trend for all the other transitions, since it appears very broad for $x = 0.0005$ and it progressively becomes steeper for $x = 0.005$ and 0.02. This trend can be attributed to its proximity to the lower temperature N*–SmA transition. In Figure 3 it is illustrated that by increasing the concentration of CdSe nanoparticles the BPI–N* transition gradually approaches the

N*–SmA anomaly. For the $x = 0.02$ mixture, in particular, the BPI–N* transition is already superimposed on the pretransitional wing of the N*–SmA transition. Hence, the supercooled BP ordering undergoes a transition into an N* phase with substantial SmA order, resulting in a much steeper BPI–N* peak compared to the $x \leq 0.005$ mixtures.

The heating runs for the CdSe mixtures of $x = 0.005$ and 0.02 are shown in Figure 4. No heating run was performed for the $x = 0.0005$ mixture, since the impact of nanoparticles on the transitions in such a low concentration was still mild. The heating runs reveal two interesting features. The first is the extended and fully reproducible BPIII broadening, which exhibits the same range among the heating and the cooling runs within a few millikelvin. The small hysteresis in the transition temperatures is due to the first-order character of the transitions. The second feature is the difference in the range of BPI as well as its stabilisation in the presence of nanoparticles. The former is shortened and the latter is weaker upon heating. This leads to the conclusion that BPI is supercooled less for the pure CE6 and more in the presence of CdSe nanoparticles.

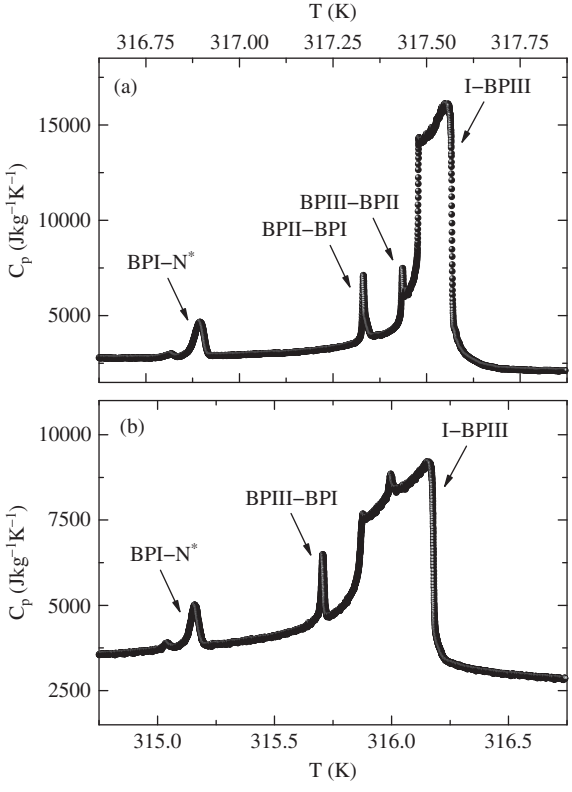

Figure 4. The $C_p(T)$ profile for the very slow heating runs performed on CE6 and CdSe mixtures: (a) $x = 0.005$; (b) $x = 0.02$.

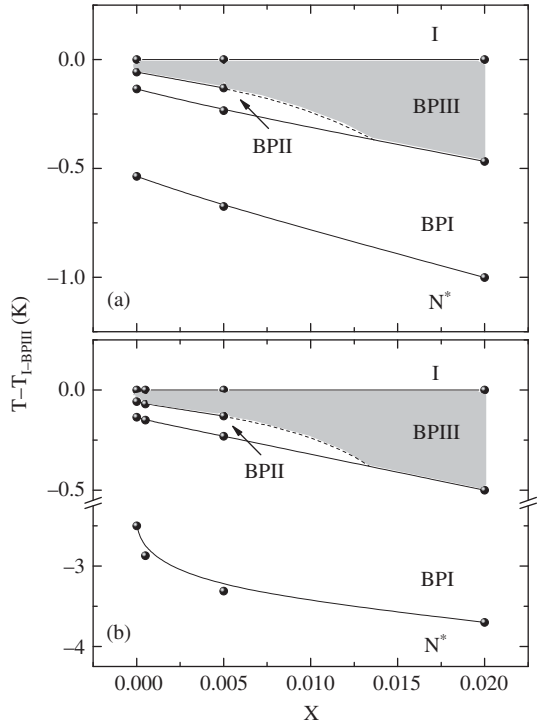

Figure 5. The T–x phase diagram upon heating (a) and cooling (b), for CE6 and its mixtures with CdSe nanoparticles. Break points have been used along the y-axis at the bottom layer in order to create the same scale for the BPIII region between the two layers and demonstrate the reproducible effect on BPIII upon heating and cooling.

The extended versus the mild broadening of BPIII and BPI phases, respectively, as well as the gradual disappearance of BPII can be pictured in the T–x phase diagrams of Figure 5 corresponding to heating (a) and cooling (b). For clarity, $T_{I-BPIII}$, which is defined as the temperature of the onset of BPIII, i.e. at the beginning of the coexistence region on the I side, has been subtracted from all of the transition temperatures. The dashed lines indicate the approximate area where BPII disappears, since it is visible for the $x \leq 0.005$ and it vanishes for $x = 0.02$. For the phase diagram based on the cooling runs we have used the transition temperatures of bulk CE6 reported in [42] as well as our microscopic observations, since only one control heating run was performed by calorimetry in the present work. Break points have been used along the y-axis of Figure 5(b) in order to achieve a common scale in the vicinity of BPIII between the upper and lower plot. In this way the full reproducibility (within a few millikelvin) of the stabilisation of BPIII upon heating and cooling is clear to the reader. This is of particular importance because it rules out the possibility of supercooling effects and refers to a thermodynamically stable state. For $x = 0.02$ the BPIII

Table 2. The enthalpy changes involved at the transitions of CE6 and its mixtures with CdSe nanoparticles. From left to right the enthalpies of the BPIII–BPII (or direct BPIII–BPI), BPII–BPI and BPI–N* transitions are given in units of J g^{-1}.

Sample	$\Delta H_{\mathrm{BPIII-BPII}}$	$\Delta H_{\mathrm{BPIII-BPI}}$	$\Delta H_{\mathrm{BPII-BPI}}$	$\Delta H_{\mathrm{BPI-N^*}}$
CE6 ($x=0$)	0.026 ± 0.003		0.045 ± 0.003	0.075 ± 0.004
$x=0.0005$	0.023 ± 0.003		0.045 ± 0.003	0.067 ± 0.006
$x=0.005$	0.022 ± 0.003		0.041 ± 0.006	0.066 ± 0.004
$x=0.02$		0.051 ± 0.003		0.063 ± 0.004

range (~0.48 K on heating and ~0.50 K on cooling) is extended by almost an order of magnitude compared to the bulk CE6 (~0.057 K). Although the absolute value of the BPIII range is still small, the stabilisation effect is striking. Hence, if applied on compounds with wider BP range close to room temperature, this method can provide wide-range BPIII which would be potentially useful for applications.

The enthalpy changes related to the conversions between the BPs are given in Table 2. For the pure sample and the smaller concentrations of nanoparticles ($x \leq 0.005$) there are two distinct transitions, BPIII–BPII and BPII–BPI, while for the larger concentration ($x=0.02$) BPII disappears and a direct BPIII–BPI transition occurs. There exists a very good agreement between the enthalpy change values ΔH derived from the heating and cooling runs of the same sample, since the applied scanning rates were slow in both cases. Nevertheless, the (slower) heating runs were used for the determination of ΔH, apart from the concentration $x=0.0005$ for which no heating run was performed. The determination of ΔH was derived from the enthalpy–temperature $H(T)$ curve. Such a curve is shown in Figure 6 for pure CE6 in the vicinity of BPs. The three insets in Figure 6 show 'close ups' of the enthalpy curve in a narrow temperature range around the BP conversions, since in the full-range plot these very narrow and sharp transitions cannot be so easily distinguished.

The enthalpy changes related to each of the BPIII–BPII (or direct BPIII–BPI), BPII–BPI and BPI–N* transitions are given in Table 2 for CE6 and all of the mixtures. It is not possible to reliably distinguish between the enthalpy changes related to the I–BPIII and the N*–SmA phase transition, owing to their proximity and the rather large pretransitional effects. Instead, the total enthalpy $\Delta H_{\mathrm{total}}$ related to all of the phase transitions occurring between the I and the SmA phase determined from the cooling runs is given for all of the mixtures in Table 3. In the same table, the enthalpy change $\Delta H_{\mathrm{BPIII-BPII-BPI-N^*}}$ (phase sequence BPIII–BPII–BPI–N* for $x \leq 0.005$) or $\Delta H_{\mathrm{BPIII-BPI-N^*}}$ (phase sequence BPIII–BPI–N* for $x=0.02$) is

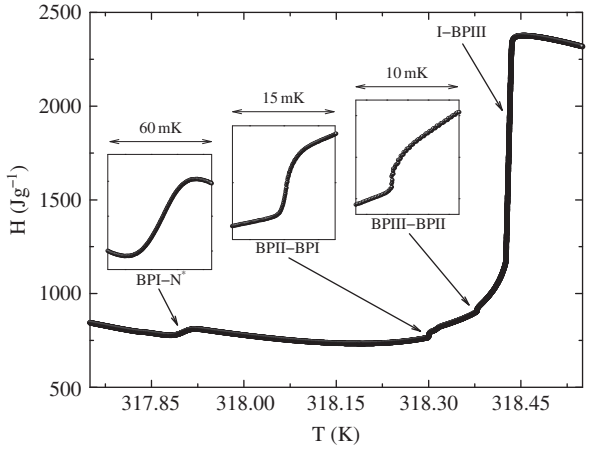

Figure 6. The enthalpy curve in the vicinity of BPs for pure CE6. The insets provide 'close ups' of the curve in the narrow temperature ranges close to each transition of 60 mK for BPI–N*, 15 mK for BPII–BPI and 10 mK for BPIII–BPII.

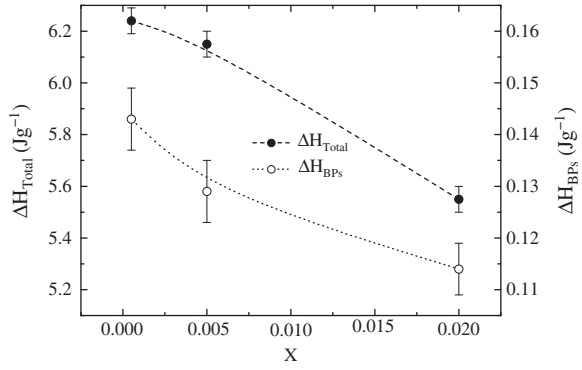

Figure 7. The evolution of the total enthalpy change ΔH_{Total} due to all of the phase transitions between the I and the SmA phase (solid symbols and the dashed line as a guide to the eye). In addition, the evolution of the enthalpy changes ΔH_{BPs} related to the conversions between the BPs is shown (open symbols and the dotted line as a guide to the eye). ΔH_{BPs} refers to either $\Delta H_{\mathrm{BPIII-BPII-BPI-N^*}}$ (for $x \leq 0.005$) or to $\Delta H_{\mathrm{BPIII-BPI-N^*}}$ (for $x=0.02$).

presented. The quantities $\Delta H_{\mathrm{Total}}$, $\Delta H_{\mathrm{BPIII-BPII-BPI-N^*}}$ (or $\Delta H_{\mathrm{BPIII-BPI-N^*}}$) monotonously decrease with the addition of CdSe nanoparticles in the mixture. Their

Table 3. The total enthalpy change related to all BP conversions and the total enthalpy change from I down to the SmA phase in units of J g^{-1} for all CE6 and CdSe mixtures.

Sample	$\Delta H_{\mathrm{BPIII-BPII-BPI-N^*}}$	$\Delta H_{\mathrm{BPIII-BPI-N^*}}$	$\Delta H_{\mathrm{Total}}$
$x = 0.0005$	0.143 ± 0.006		6.24 ± 0.05
$x = 0.005$	0.129 ± 0.006		6.15 ± 0.05
$x = 0.02$		0.114 ± 0.005	5.55 ± 0.05

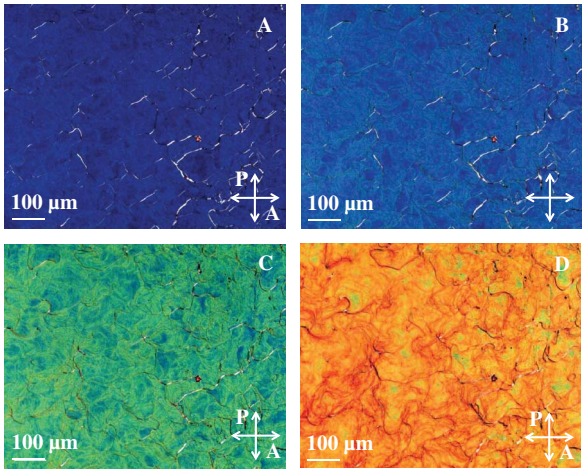

Figure 8. Polarising microscopy images in the range of the BPs of pure CE6 upon cooling of the sample (A, B, C, D in order of decreasing temperature).

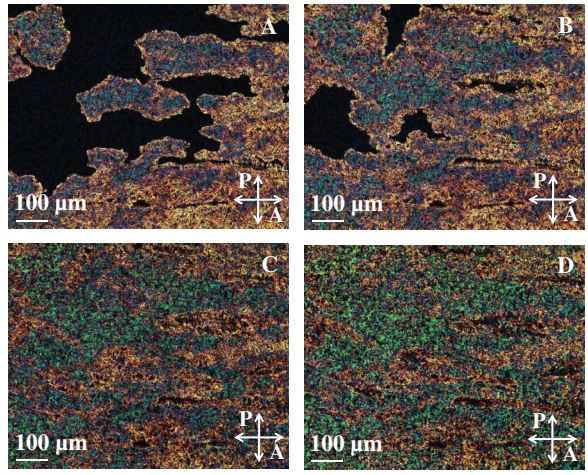

Figure 9. Polarising microscopy images of the $x = 0.02$ sample upon cooling. The top part (images A and B in order of decreasing temperature) corresponds to the gradual growth of BPIII inside the I phase. The bottom part (images C and D in order of decreasing temperature) corresponds to the evolution of the texture along the BPIII–BPI phase transition.

evolution, which is graphically represented in Figure 7, is close to linear.

Complementary microscopic observations have been performed in the vicinity of BPs for the pure CE6. Owing to the very small range of BPs in the pure CE6, which is of the order of the temperature stability of the heating stage (i.e. $\pm$ 0.1 K) it was practically impossible to stabilise the sample at temperatures within the BPs. Instead, the sample was cooled rather fast from the I phase and then a sequence of images was collected. In Figure 8 four microscopic images (A, B, C and D, in order of decreasing temperature) for pure CE6 can be seen at the three BPs. The gradual change of colour, corresponding to the different BPs, can be nicely observed.

Microscopic observations were also performed for the $x = 0.02$ mixture. Since the BPs of this mixture exhibit a significantly wider temperature range compared to pure CE6, it was easier to probe the evolution of phases. Nevertheless, the images were darker compared to those of pure CE6 due to the presence of the CdSe nanoparticles. In the top panel of Figure 9 (images A and B, in order of decreasing temperature) the gradual growth of BPIII inside the dark regions of the I phase can be clearly observed. Likewise, in the bottom panel of Figure 9 (images C and D, in order of decreasing temperature) the gradual change of the texture colour between BPIII and BPI of the same sample can be followed.

As demonstrated in the present work, the addition of surface-functionalised CdSe nanoparticles to CE6 affects strongly BPIII and weakly BPI. In contrast, other means of stabilisation have been reported to affect mostly BPI [23, 25]. The apparent widening of BPI observed in our measurements is attributed to supercooling. This implies that particular attention must be paid to exclude supercooling phenomena in the studies of BPs. The combination of various experimental techniques in studies of BPs as well as the performance of heating and cooling runs are valuable tools in this direction.

Our experimental findings suggest that the addition of CdSe nanoparticles produces a qualitatively similar phase diagram to that for an increasing chirality strength [15]. Moreover, a plausible scenario dealing with the trapping of the CdSe nanoparticles in the disclination lines has been proposed recently [36] in

order to account for the widening of BPIII. Note that these two mechanisms could be related. Namely, the dimensionless chirality strength is expressed as a ratio of the representative elastic and condensation free energy density terms. It is assumed that the nanoparticles assemble at the disclination cores and, consequently, they reduce the condensation free energy penalty (i.e. the costs to melt the liquid crystal orientational ordering). Therefore, the effective condensation free energy of the system is reduced, the elastic penalty remains roughly the same and the chirality strength is increased [36].

Other issues that might play an important role in the stabilisation of BPs, which have so far been inadequately explored, are the size, the shape and the self-organisation of the nanoparticles [43]. In a recent work it was reported that silica aerosil type 300 nanoparticles do not have a comparable effect to nanoparticles of CdSe for BPs of the chiral liquid crystal CE8. Yet, it is not clear whether this is related to the different surface treatment of the nanoparticles (hydrophilic for aerosil 300 versus hydrophobic for the CdSe), to the different size (7.0 nm for aerosil 300 versus 4.5 nm for CdSe), to the fact that aerosils form adaptive networks while CdSe does not or to some interplay of all the above. We believe that further experimental and theoretical studies are needed to gain a profound understanding of the mechanisms behind BP stabilisation.

4. Conclusions

Various homogeneous mixtures of liquid crystal CE6 with CdSe nanoparticles ($2R \sim 4.5$ nm) bearing a hydrophobic coating have been investigated by high-resolution calorimetry and optical polarising microscopy. It has been demonstrated that with an increase of the concentration of nanoparticles, BPIII is greatly stabilised, BPII gradually vanishes and BPI is weakly affected. In particular, the BPIII range appears at the same temperature interval upon heating and cooling, within a few millikelvin. The width of its range appears impressively stable among heating and cooling runs, although the absolute temperatures are slightly shifted due to hysteresis. The limited widening of BPI, more pronounced on cooling, is mainly attributed to supercooling effects which are enhanced by the presence of nanoparticles.

5. Acknowledgements

This work was supported by the Slovenian Research Agency (program P1-0125 and projects J1-9368 and J1-2015). GC acknowledges the support of the FWO (Project 'AVISCO' nr. G.0230.07) and the Research Fund of K. U. Leuven for 2009, and the EN FIST Centre of Excellence (Dunajska 156, SI-1000 Ljubljana, Slovenia) for finance during 2010. EK acknowledges the Graduate Fellowship Program of N.C.S.R. 'Demokritos'.

References

[1] Reinitzer, F. *Monatsh. Chem.* **1888**, *9*, 421–441 [Engl. transl. Weiss, A. *Liq. Cryst.* **1989**, *5*, 7–8].
[2] Crooker, P.P. *Mol. Cryst. Liq. Cryst.* **1983**, *98*, 31–45.
[3] Barbet-Massin, R.; Cladis, P.E.; Pieranski, P. *Phys. Rev. A: At., Mol., Opt. Phys.* **1984**, *9*, 118–120.
[4] Keyes, P.H. *Phys. Rev. Lett.* **1990**, *65*, 436–439.
[5] Dubois-Violette, E.; Pansu, B.; Pieranski, P. *Mol. Cryst. Liq. Cryst.* **1990**, *192*, 221–237.
[6] Koistinen, E.P.; Keyes, P.H. *Phys. Rev. Lett.* **1995**, *74*, 4460–4463.
[7] Collings, P.J. *Phys. Rev. A: At., Mol., Opt. Phys.* **1984**, *30*, 30–33.
[8] Tanimoto, K.; Crooker, P.P.; Koch, G.C. *Phys. Rev. A: At., Mol., Opt. Phys.* **1985**, *32*, 32–34.
[9] Armitage, D.; Price, F.P. *J. Phys. (Paris) Colloq.* **1975**, *98*, (C1)133–136.
[10] Thoen, J. *Phys. Rev. A: At., Mol., Opt. Phys.* **1988**, *37*, 37–42.
[11] Brazovskii, S.A.; Dmitriev, S.G. *Zh. Eksp. Teor. Fiz.* **1975**, *69*, 979–989.
[12] Meiboom, S.; Sethna, J.P.; Anderson, P.W.; Brinkman, W.F. *Phys. Rev. Lett.* **1981**, *46*, 1216–1219.
[13] Grebel, H.; Hornreich, R.M.; Shtrikman, S. *Phys. Rev. A: At., Mol., Opt. Phys.* **1983**, *28*, 1114–1138.
[14] Belyakov, V.A.; Dmitrienko, V.E. *Liq. Cryst.* **1989**, *5*, 839–846.
[15] Bowling, M.B.; Collings, P.J.; Booth, C.J.; Goodby, J.W. *Phys. Rev. E: Stat., Nonlinear, Soft Matter Phys.* **1993**, *48*, 4113–4115.
[16] Kutnjak, Z.; Garland, C.W. *Phys. Rev. Lett.* **1995**, *74*, 4859–4862.
[17] Kutnjak, Z.; Garland, C.W.; Schatz, C.G.; Collings, P.J.; Booth, C.J.; Goodby, J.W. *Phys. Rev. E: Stat., Nonlinear, Soft Matter Phys.* **1996**, *53*, 4955–4963.
[18] Anisimov, M.A.; Agayan, V.A.; Collings, P.J. *Phys. Rev. E: Stat., Nonlinear, Soft Matter Phys.* **1998**, *57*, 582–595.
[19] Cao, W.; Munoz, A.; Palffy-Muhoray, P.; Taheri, B. *Nat. Mater.* **2002**, *1*, 111–113.
[20] Rao, L.H.; Ge, Z.B.; Wu, S.T.; Lee, S.H. *Appl. Phys. Lett.* **2009**, *95*, 231101.
[21] Liu, H.Y.; Wang, C.T.; Hsu, C.Y.; Lin, T.H.; Liu, J.H. *Appl. Phys. Lett.* **2010**, *96*, 121103.
[22] Kitzerow, H.S.; Schmid, H.; Ranft, A.; Heppke, G.; Hikmet, A.M.; Lub, J. *Liq. Cryst.* **1993**, *14*, 911–116.
[23] Kikuchi, H.; Yokota, M.; Hisakado, Y.; Yang, H.; Kajiyama, T. *Nat. Mater.* **2002**, *1*, 64–68.
[24] Nakata, M.; Takanishi, Y.; Watanabe, J.; Takezoe, H. *Phys. Rev. E: Stat., Nonlinear, Soft Matter Phys.* **2003**, *68*, 041710.
[25] Coles, H.J.; Pivnenko, M.N. *Nature (London, UK)* **2005**, *436*, 997–1000.
[26] Hisakado, Y.; Kikuchi, H.; Nagamura, T.; Kajiyama, T. *Adv. Mater. (Weinheim, Ger.)* **2005**, *17*, 96–98.
[27] Alexander, G.P.; Yeomans, J.M. *Phys. Rev. E: Stat., Nonlinear, Soft Matter Phys.* **2006**, *74*, 061706.
[28] Yoshizawa, A.; Iwamochi, H.; Segawa, S.; Sato, M. *Liq. Cryst.* **2007**, *34*, 1039–1044.

[29] Noma, T.; Ojima, M.; Asagi, H.; Kawahira, Y.; Fujij, A.; Ozaki, M. *J. Surf. Sci. Nanotech.* **2008**, *6*, 17–20.
[30] Ravnik, M.; Alexander, G.P.; Yeomans, J.M.; Žumer, S. *Faraday Discus.* **2010**, *144*, 159–169.
[31] Fukuda, J.; Žumer, S. *Phys. Rev. Lett.* **2010**, *104*, 017801.
[32] Castles, F.; Morris, S.M.; Terentjev, E.M.; Coles, H.J. *Phys. Rev. Lett.* **2010**, *104*, 157801.
[33] Yoshizawa, A.; Kogawa, Y.; Kobayashi, K.; Takanishi, Y.; Yamamoto, J. *J. Mater. Chem.* **2009**, *19*, 5759–5764.
[34] Iwamoshi, H.; Hirose, T.; Kogawa, Y.; Yoshizawa, A.; *Chem. Lett.* **2010**, *39*, 170–171.
[35] Yoshida, H.; Tanaka, Y., Kawamoto, K.; Kubo, H.; Tsuda, T.; Fujii, A.; Kuwabata, S.; Kikuchi, H.; Ozaki, M. *Appl. Phys. Express* **2009**, *2*, 121501.
[36] Karatairi, E.; Rožič, B., Kutnjak, Z.; Tzitzios, V.; Nounesis, G.; Cordoyiannis, G.; Glorieux, C.; Thoen, J.; Kralj, S. *Phys. Rev. E: Stat., Nonlinear, Soft Matter Phys.* **2010**, *81*, 041703.
[37] Yang, D.K.; Crooker, P.P. *Phys. Rev. A: At., Mol., Opt. Phys.* **1987**, *35*, 4419–4423.
[38] Voets, G.; Van Dael, W. *Liq. Cryst.* **1993**, *14*, 61–27.
[39] Tzitzios, V.; Georgakilas, V.; Zafiropoulou, I.; Boukos, N.; Basina, G.; Niarchos, D.; Petridis, D. *J. Nanosci. Nanotechno.* **2008**, *8*, 3117–3122.
[40] Thoen, J.; Marynissen, H.; Van Dael, W. *Phys. Rev. A: At., Mol., Opt. Phys.* **1982**, *26*, 2886–2905.
[41] Thoen, J.; Cordoyiannis, G.; Glorieux, C. *Liq. Cryst.* **2009**, *36*, 669–684.
[42] Voets, G. Ph.D. Thesis, Katholieke Universiteit Leuven, 1993.
[43] Ravnik, M. *Oral Presentation 0–50*, 10th European Conference on Liquid Crystals, Colmar, France, 2009.